J. Phys. D: Appl. Phys. **32** (1999) 2833–2840. Printed in the UK PII: S0022-3727(99)04369-7

Effect of elastic distortions on solid-state amorphization at grain boundaries and dislocations

Ilya A Ovid'ko and Anna B Reizis

Laboratory for Theory of Defects in Materials, Institute for Problems of Mechanical Engineering, Russian Academy of Sciences, Bolshoj 61, Vas. Ostrov, St. Petersburg 199178, Russia

E-mail: ovidko@def.ipme.ru

Received 18 May 1999, in final form 3 August 1999

Abstract. Two theoretical models are proposed, which describe solid-state amorphizing transformations at, respectively, grain boundaries and dislocations in crystalline solids. In the framework of the former model, the driving force for the formation of an amorphous intergranular layer is revealed and estimated, which is related to changes in the elastic energy density of a conventional grain boundary that transforms into the amorphous layer. The second model describes nucleation of the amorphous phase at the cores of lattice and interfacial dislocations as a process associated with the special splitting of such dislocations. In the framework of the model, the special role of elastic distortions in solid-state amorphization at dislocation cores is revealed and examined.

1. Introduction

Solid-state amorphizing transformations or, in other terms, crystal-to-glass transitions are the subject of intensive studies (for a review see [1–6]). In particular, the solid-state amorphizing transformations occur in multilayer coatings consisting of alternate metallic layers, in mechanically alloyed metallic powders, in irradiated crystals, in metallic alloys under high-strain deformation, and in ceramics at sintering processes.

Up to now, physical micromechanisms of the solid-state amorphization have not been unambigiously recognized. At the same time, such micromechanisms are of great interest for the development of technologies related to the solid-state amorphizing transformations. In experimental studies the role of defects has been revealed to be very important in amorphization phenomena in crystals. In particular, it has been experimentally observed that the amorphous phase commonly nucleates at interphase and (inter)grain boundaries [7–9] and, sometimes, at interfacial and lattice dislocations [10, 11]. In order to take into account the important role of defects in the solid-state amorphization, several theoretical models have been proposed describing such amorphization micromechanisms as the splitting of disclinations at triple junctions of grain boundaries [12, 13], special diffusion-induced grain boundary migration [14], amorphization in regions with high-density ensembles of point defects [15, 16], and deformation-induced splitting of grain boundaries intersected with pile-ups of lattice dislocations [17]. Also, the thermodynamic analysis of the effect of interfaces on the solid-state amorphization in metallic multilayer coatings has been performed by Benedictus *et al* [18]. The main aim of this paper is to suggest and theoretically describe the amorphization micromechanisms which are the elastic-energy-decrease-induced splitting of grain boundaries and the special splitting of lattice and interfacial dislocations.

2. Elastic energy of amorphous intergranular boundaries

Elastic distortions induced by a grain boundary are effectively described as those induced by grain-boundary dislocations (GBDs) arranged in a wall-like ensemble [19–21]. Such GBDs exist in any grain boundary for geometric reasons; more precisely, GBDs play the role as elemental carriers of grain-boundary misorientation. If a grain boundary is formed at quasi-equilibrium conditions, interspacings between GBDs and their Burgers vectors are strictly caused by geometric parameters (misorientation, etc) of the boundary. If a grain boundary is formed at non-equilibrium conditions (say, by hot-pressing methods), additional GBDs exist in the boundary that are disorderedly distributed and induce high elastic distortions, see for example [20].

In the light of the GBD picture, we think the formation of amorphous intergranular boundaries as a process associated with a re-distribution of GBDs, leading to a decrease of their elastic energy. Actually, the disordered amorphous structure, in contrast to equilibrium structures of non-amorphized grain boundaries, does not impose strict geometric restrictions on

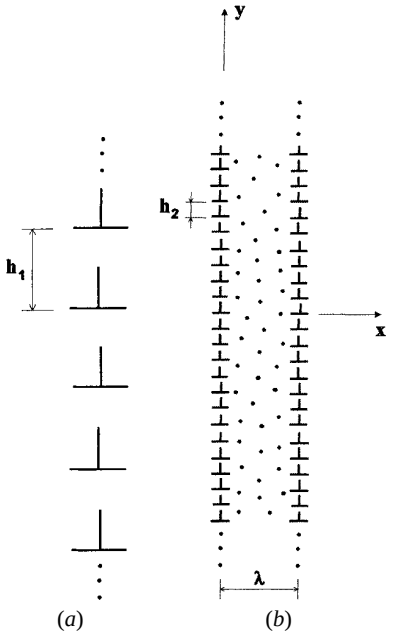

Figure 1. Configurations of GBDs in (*a*) non-amorphized boundary and (*b*) amorphous boundary, in which case the amorphous film (dotted region) is formed between two dislocation walls.

the spatial distribution of GBDs. This allows GBDs to be arranged in amorphous boundaries in a way to decrease their elastic energy in comparison with the elastic energy of GBDs in 'equilibrium' non-amorphized boundaries.

In order to estimate the difference in the elastic energy density between amorphous and non-amorphized boundaries, hereinafter we will model in the first approximation a non-amorphized grain boundary as a periodic wall of GBDs with period h_1 (figure 1(*a*)), and amorphous boundary as two periodic walls of GBDs, each having period h_2, in which case the amorphous film is located between these two walls (figure 1(*b*)). GBDs belonging to dislocation configurations in non-amorphized (figure 1(*a*)) and amorphous (figure 1(*b*)) boundaries are supposed to be characterized by Burgers vectors $\boldsymbol{b_1}$ and $\boldsymbol{b_2}$, respectively, that satisfy the following equality: $\boldsymbol{b_1}/h_1 = 2\boldsymbol{b_2}/h_2$. In other words, the dislocation charge per unit of boundary length is the same for the model configurations of GBDs in question (figure 1).

In the framework of our model, the difference ΔW^{el} between the elastic energy densities of non-amorphized and amorphous boundaries is as follows:

$$\Delta W = W_1 - W_2. \tag{1}$$

Here W_1 and W_2 are the elastic energy densities of the configurations of GBDs, shown in figures 1(*a*) and 1(*b*), respectively. The elastic energy density W_1 of the GBD wall (figure 1(*a*)) is as follows [22]:

$$W_1 = \frac{Gb_1^2}{4\pi(1-\nu)h_1}\left[\frac{\pi r_0}{h_1}\coth\frac{\pi r_0}{h_1} - \ln\left(2\sinh\frac{\pi r_0}{h_1}\right)\right]. \tag{2}$$

where G denotes the shear modulus, ν the Poisson ratio, and r_0 the dislocation core radius†.

Let us consider the elastic energy density W_2. Following Mura's method [23], the elastic energy density W_2 can be calculated as follows:

$$W_2 = -\frac{1}{2}\int_S \sigma_{ij}\beta_{ij}^* \,\mathrm{d}S' \tag{3}$$

where σ_{ij} denotes the stress field, β_{ij}^* the plastic distortion and S the surface at which the displacement jump occurs (for more details, see appendix A). The plastic distortion of an edge dislocation is defined as

$$\beta_{ij}^* = \delta_i(S)\{-b_j\} \tag{4}$$

where $\delta_i(S) = \int_S \delta(\boldsymbol{r} - \boldsymbol{r}')\,\mathrm{d}S'$ with $\delta(\boldsymbol{r} - \boldsymbol{r}')$ being the three-dimensional δ-function, $\boldsymbol{r}$ denotes the coordinates of the surface S, $\boldsymbol{r}'$ is the integration coordinate and b_j is the jth component of Burgers vector of the dislocation.

Since the configuration of GBDs in question (figure 1(*b*)) is periodic, it is sufficient to calculate the elastic energy density of a GBDs configuration fragment with a length equal to period h_2. In these circumstances, the plastic distortion β_{ij}^* is defined as the sum of the plastic distortions of two dislocations that exist in the choosen GBDs configuration fragment, namely the dislocation located at the point ($x = 0$, $y = 0$) and the dislocation located at the point ($x = \lambda$, $y = 0$) (see figure 1(*b*)), where λ denotes the distance between the dislocation walls or, in other words, the thickness of the amorphous intergranular boundary.

The stress field is the sum of stress fields induced by the two dislocation walls (figure 1(*b*)), that is

$$\sigma_{ij} = \sigma_{ij}^{(1)}(x, y) + \sigma_{ij}^{(1)}(x - \lambda, y) \tag{5}$$

with $\sigma_{ij}^{(1)}$ being the stress field of one of the dislocation walls. Following [11], the field $\sigma_{ij}^{(1)}$ is as follows:

$$\begin{aligned}
\sigma_{xx}^{(1)} &= -\frac{Gb}{2\pi(1-\nu)h_2}\pi\sin 2\pi y^* \\
&\quad\times\frac{\cosh 2\pi x^* - \cos 2\pi y^* + 2\pi x^*\sinh 2\pi x^*}{(\cosh 2\pi x^* - \cos 2\pi y^*)^2} \\
\sigma_{yy}^{(1)} &= -\frac{Gb}{2\pi(1-\nu)h_2}\pi\sin 2\pi y^* \\
&\quad\times\frac{\cosh 2\pi x^* - \cos 2\pi y^* - 2\pi x^*\sinh 2\pi x^*}{(\cosh 2\pi x^* - \cos 2\pi y^*)^2} \\
\sigma_{xy}^{(1)} &= \frac{Gb}{2\pi(1-\nu)h_2}2\pi^2 x^*\frac{\cosh 2\pi x^*\cos 2\pi y^* - 1}{(\cosh 2\pi x^* - \cos 2\pi y^*)^2} \\
\sigma_{zz}^{(1)} &= \nu(\sigma_{xx} + \sigma_{yy}) \\
\sigma_{xz}^{(1)} &= \sigma_{yz}^{(1)} = 0
\end{aligned} \tag{6}$$

† In general, the energy of GBD cores contributes to the elastic energy of the configuration of GBDs. However, the atomic structures of both conventional and amorphous intergranular boundary phases are characterized by rather low values of density, in which case the contribution of GBDs cores to the elastic energy is low. In addition, the configurations of GBDs, shown in figures 1(*a*) and 1(*b*), have the same sum dislocation charge (Burgers vector). This causes only a small difference between the contributions of GBD cores to the elastic energy densities of these configurations. At the same time, namely the difference between the elastic energy densities of the configurations of GBDs is of interest in context of this paper. In these circumstances, hereinafter in our calculations we will neglect the contributions of GBD cores to the elastic energy densities.

where $x^* = x/h_2$ and $y^* = y/h_2$ are relative coordinates.

With (4)–(6) substituted to (3), we obtain the following formula for W_2:

$$W_2 = \frac{Gb_2^2}{4\pi(1-\nu)h_2}\left[2f\left(\frac{\pi r_0}{h_2}\right) + f\left(\pi\frac{r_0+\lambda}{h_2}\right) + f\left(\pi\frac{r_0-\lambda}{h_2}\right)\right]. \quad (7)$$

Here $f(\alpha) = \alpha\coth\alpha - \ln|2\sinh\alpha|$.

From formulae (2) and (7) we find a dependence of $\Delta W^{el} = W_2 - W_1$ on the boundary thickness λ, which is shown in figure 2 (in units of $Gr_0/[4\pi(1-\nu)]$) for $h_2 = 2r_0$ and some characteristic values of parameters b_1 and b_2. Its specific feature is that ΔW^{el} is tentatively constant for $\lambda > h_2$ (see figure 2). This is related to the fact that the two walls of dislocations (figure 1) do not elastically interact with each other, if the interspacing λ between them is higher than h_2, the interspacing between neighbouring dislocations in each wall, which (following to the theory of dislocations [22]) also plays the role as the screening length of stress fields of dislocations belonging to a dislocation wall.

3. Role of elastic distortions in solid-state amorphization at grain boundaries

Thus, in our model, the decrease ($-\Delta W^{el}$) in the elastic energy causes the basic driving force for the transformation of a conventional grain boundary into an amorphous intergranular layer (figure 3). There are also other contributions to the change of the total free energy (or another relevant thermodynamic potential) of the system, that are related to the amorphizing transformation (figure 3). So, such a transformation is accompanied by the formation of two crystal/glass interfaces, each of them characterized by energy density W_{int} (per unit area of interface). Following [24],

$$W_{int} \approx \varepsilon_{a-c}\kappa \quad (8)$$

where ε_{a-c} denotes the difference between the free-energy densities of the amorphous and crystalline phases, and κ is the characteristic spatial scale of structural inhomogeneities in the amorphous phase. The value of $2W_{int}$ serves as an energetic characteristic of the amorphizing transformation (figure 3).

To deal with another characteristic, hereinafter we assume that the transformation of a conventional grain boundary into an amorphous intergranular layer occurs at its initial stage in a jump-like way, with the thickness λ_0 of the conventional boundary abruptly changing into the thickness $\lambda_0 + \Delta\lambda$ of the amorphous layer (figure 3). This transformation results, in particular, in both the crystal-to-glass transition occuring within the region with the thickness $\Delta\lambda$ and the grain-boundary-phase-to-glass transition occuring within the region with the thickness λ (figure 3). Since the free-energy densities of the grain boundary phase and the glassy phase are close, the transitions in question are approximately characterized by the following contribution

$$\Delta W_{a-c} \approx \Delta\lambda\varepsilon_{a-c} \quad (9)$$

Table 1. ΔW for various values of b_1 and b_2.

Values of b_1 and b_2	ΔW ($G\,a$)
$b_2 = a/10$, $b_1 = 6b_2$	−0.164
$b_1 = 10b_2$	−0.154
$b_1 = 20b_2$	−0.120
$b_2 = a/20$, $b_1 = 6b_2$	−0.170
$b_1 = 10b_2$	−0.167
$b_1 = 20b_2$	−0.158

to the total free-energy density per unit area of the amorphized boundary.

Thus the free-energy decrease related to the amorphizing transformation at its initial (jump-like) stage (figure 3) is as follows:

$$\Delta W \approx W_1 - W_2|_{\lambda=\lambda_0+\Delta\lambda} - (2\kappa + \Delta\lambda)\varepsilon_{a-c} \quad (10)$$

where W_1 and $W_2(\lambda)$ are given by formulae (2) and (7), respectively. The amorphizing transformation (figure 3) occurs as an energetically profitable transformation, if $\Delta W > 0$. When $\Delta W < 0$, the amorphizing transformation is energetically forbidden.

In order to estimate ΔW, let us discuss entity ε_{a-c} which figures on the right-hand side of (10). In doing so, we distinguish the two following situations:

(1) *The initial crystalline phase contains 'ordinary' (small or intermediate) density of defects near the grain boundary. The chemical composition of the boundary and its vicinity is constant and close to that of the adjacent crystalline grains*. In this situation (which is rather ordinary in crystals) the difference ε_{a-c} between the free-energy densities of the amorphous and crystalline phases ranges from $G/83$ to $G/63$ (see [25] and references therein, in which ε_{a-c} was measured for glass-to-crystal transitions resulting in crystals with small densities of defects), where G is the shear modulus. With this taken into account, for characteristic values of parameters $\kappa \approx 1.5\times10^{-9}$ m (see [26] and references therein), $\lambda_0 \approx 3a$ (where $a \approx 3\times10^{-10}$ m is the crystal lattice parameter), $\Delta\lambda \approx 2a$, $r_0 \approx a$, $\nu = \frac{1}{3}$, $\varepsilon_{a-c} = G/70$, $b_2 \approx a/10$ and $a/20$, and $b_1 = 6b_2, 10b_2$, and $20b_2$ from (2), (7), and (10) we find $\Delta W < 0$ (see table 1). As a corollary, the amorphizing transformation (figure 3) is energetically forbidden in the discussed situation.

(2) *The initial crystalline phase contains a high density of defects and/or the chemical composition of a grain boundary and its vicinity is different from that of the adjacent crystalline grains*. Such a situation occurs, in particular, in crystalline solids under irradiation treatment and high-strain deformation that produce high-density ensembles of defects. The presence of high-density ensembles of irradiation- or deformation-produced defects essentially increases the free-energy density of the crystalline phase, in which case this density becomes close to the free-energy density of the amorphous phase. As a result, ε_{a-c} in solids with high densities of defects is essentially smaller than ε_{a-c} in solids with 'ordinary' (small or intermediate) densities of defects. Also, the discussed situation (2) comes into play in cintered ceramics, where the chemical composition of

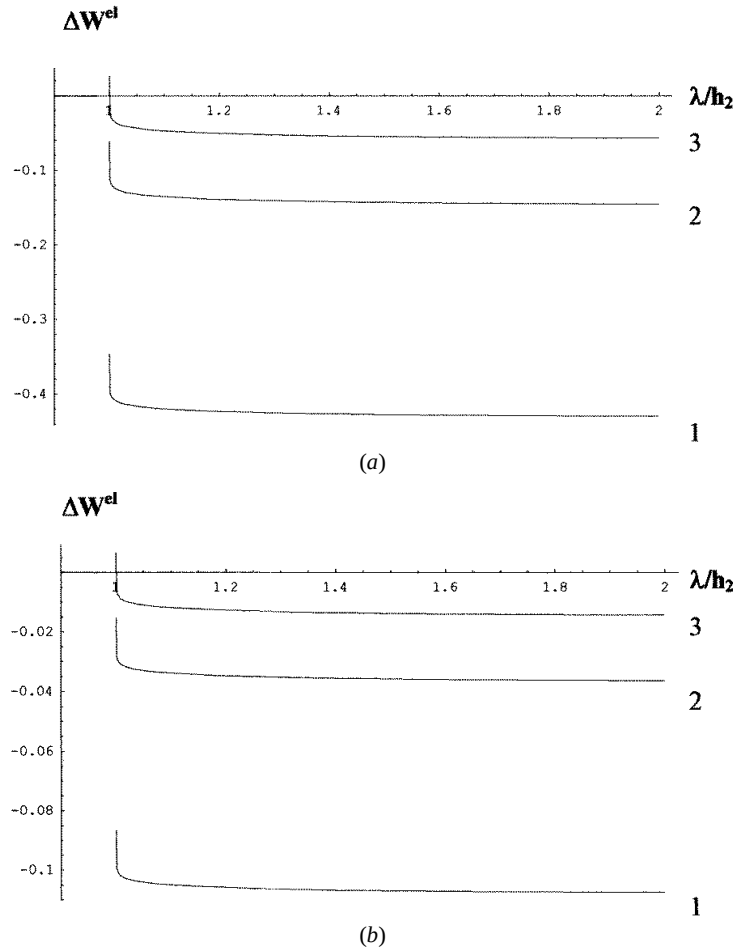

Figure 2. Dependence of ΔW on λ, (*a*) for $b_2 = r_0/10$ and (*b*) for $b_2 = r_0/20$. Curves 1, 2 and 3 correspond to values of $b_1 = 6b_2$, $10b_2$ and $20b_2$, respectively.

the grain boundary phase is different from that of the bulk phase, as well as in multilayer metallic coatings, in which intensive grain boundary diffusion causes highly varied spatial inhomogeneities of the chemical composition [1–4]. In these circumstances, the value of ε_{a-c} characterizing grain boundaries and their vicinities can be essentially lower than the values of ε_{a-c} in situation (1). More than that, due to diffusional mixing, the value of ε_{a-c} can even be less than zero, which specifies the material in and near grain boundaries in multilayer metallic coatings [1–4]. With this taken into account, for characteristic values of the parameters $\lambda_0 \approx 3a$, $\Delta\lambda \approx 2a$, $\kappa \approx 5a$ ($\approx 1.5 \times 10^{-9}$ m), $r_0 \approx a$, $\nu \approx 1/3$, and $b_2 \approx a/10$ and $a/20$, from (2), (7), and (10) we find dependences of ΔW on ε_{a-c}, which are shown in figure 4. $\Delta W(\varepsilon_{a-c}) > 0$, in some ranges of the parameters (see figure 4), in which case the transformation of a conventional grain boundary into an amorphous intergranular layer (figure 3) is energetically profitable.

Now let us turn to the analysis of a continuous spreading of an amorphous intergranular layer, after the layer has been initially formed in the jump-like way. The spreading occurs continuously and is featured by a continuous change (increase) of the thickness λ of the amorphous layer. In these circumstances, the driving force for the spreading, related to

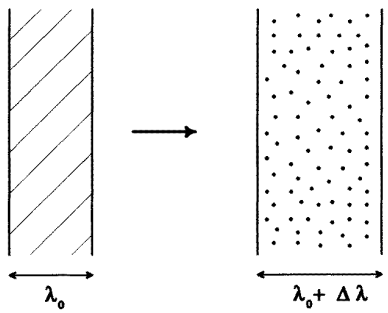

Figure 3. The starting stage of the transformation of a conventional grain boundary (with thickness λ_0) into an amorphous intergranular layer (with thickness $\lambda_0 + \Delta\lambda$).

decrease $\Delta W^{el} = W_2 - W_1$ in the elastic energy, is naturally defined as

$$F^{el} = -\left(\frac{\mathrm{d}\Delta W^{el}}{\mathrm{d}\lambda}\right) = \frac{Gb_2^2\pi^2}{4\pi(1-\nu)h_2^2}\left[\frac{r_0+\lambda}{h_2} \times \operatorname{csch}\left(\pi\frac{r_0+\lambda}{h_2}\right)^2 - \frac{r_0-\lambda}{h_2}\operatorname{csch}\left(\pi\frac{r_0-\lambda}{h_2}\right)^2\right]. \quad (11)$$

The driving force F^{el} related to decrease in the elastic energy is high at $\lambda \leqslant h_2$ and rather low at $\lambda > h_2$, because the value of ΔW^{el} is highly sensitive to λ in the range of $\lambda > h_2$ and

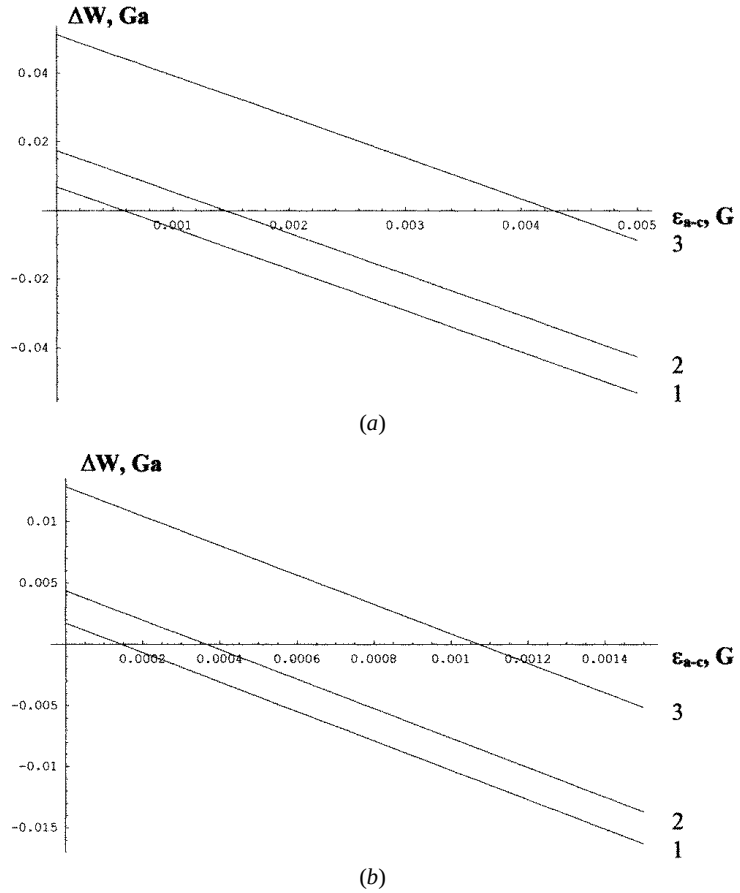

Figure 4. Dependences of ΔW on ε_{a-c} for (*a*) $b_2 = a/10$ and (*b*) $b_2 = a/20$. Curves 1, 2 and 3 correspond to values of $b_1 = 6b_2$, $10b_2$ and $20b_2$, respectively.

is weakly dependent on λ in the range $\lambda > h_2$ (see figure 2). As a corollary, the force F^{el} plays the important role as a driving force for the spreading of an amorphous layer, but only at the formation stage characterized by values of $\lambda \leqslant h_2$. For $\lambda > h_2$, F^{el} stops being essential as a driving force, in which case another thermodynamic force F' mainly affects the spreading of an amorphous layer.

Let us briefly discuss the force F'. This force originates from spreading-induced changes in both the crystal/glass interfacial-energy density $2\kappa\varepsilon_{a-c}$ and the amorphous-layer energy density $\lambda\varepsilon_{a-c}$, but not taking into account changes in the elastic energy density. Since ε_{a-c}, generally speaking, is dependent on λ (due to spatial inhomogeneities of the chemical composition), the force $\tilde{F}$ in its general form is defined as

$$F'(\lambda) \approx -\varepsilon_{a-c}(\lambda) - (2\kappa + \lambda)\frac{\mathrm{d}\varepsilon_{a-c}(\lambda)}{\mathrm{d}\lambda} \qquad (12)$$

The thermodynamic force F' can be either a driving or hampering force (either >0 or <0) for the spreading of an amorphous layer in different solid systems, depending on the structural characteristics and chemical composition of such systems. A detailed (cumbersome and labour-consuming) analysis of F' is beyond the scope of this paper which is devoted to the examination of the role of elastic distortions in solid-state amorphizing transformations.

4. Role of elastic distortions in solid-state amorphization at lattice and interfacial dislocations

The amorphous phase was observed experimentally to be nucleated at lattice dislocation cores in quartz under irradiation treatment [10]. Also, it has been revealed experimentally that amorphous SiO_2 precipitates are formed at grain boundary steps (being sources of stress fields) in Si bicrystals under thermal treatment [11]. In order to explain these experimental data, in this section we suggest a model that describes the splitting of dislocations as an amorphization micromechanism. In doing so, special attention is paid to the role of elastic distortions in such a splitting process.

Within the framework of the proposed model, a pre-existent, either lattice or interfacial, dislocation with Burgers vector $\vec{B}$ splits into a cylinder-like array of dislocations with small Burgers vectors, in which case the core of the pre-existent dislocation, in fact, spreads into the cylinder-like region (figure 5). Since the resultant dislocations with small Burgers vectors are partial, the cylinder-like region is disordered and naturally treated as a nucleus of the amorphous phase.

The basic driving force for the amorphizing splitting of a dislocation is related to a splitting-induced decrease $\Delta\tilde{W}^{el}$ in the elastic energy of the dislocation. The hampering forces for the splitting are commonly associated with the

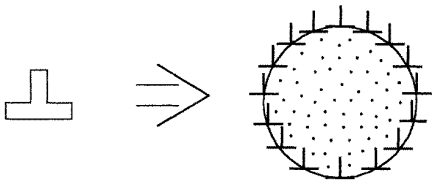

Figure 5. The splitting of a dislocation into a cylinder-like ensemble of dislocations with small Burgers vectors, which is accompanied by the formation of the amorphous (dotted) region, the core of the split dislocation.

excess energy density $\tilde{W}_c$ of the amorphous core of the split dislocation and with the energy density $\tilde{W}_{int}$ of the crystal/glass interface whose formation results from the splitting (figure 5).

Let us consider the splitting-induced decrease in the elastic energy density, which can be divided into the three terms

$$\Delta\tilde{W}^{el} = \tilde{W}_r - \tilde{W}_p + \tilde{W}_{d-d}. \tag{13}$$

Here $\tilde{W}_p$ and $\tilde{W}_r$ are the proper energy densities of the pre-existent dislocation and that of the ensemble of the resultant dislocations with small Burgers vectors. $\tilde{W}_{d-d}$ denotes the energy density of the interaction between the resultant dislocations.

The proper energy density of the pre-existent dislocation with Burgers vector $\vec{B}$ is given by the following standard formula (e.g. [22])

$$\tilde{W}_p \approx \frac{GB^2}{4\pi(1-\nu)}\left(\ln\frac{R}{r_0} + Z\right) \tag{14}$$

where G denotes the shear modulus, ν the Poisson ratio, Z the factor taking into account the contribution of the pre-existent dislocation core to its energy ($Z \approx 1$), r_0 the dislocation core radius (assumed to be close to a, the lattice parameter), and R denotes the screening length of the dislocation stress field. (The value of R depends on the spatial distribution of sources of stresses near the pre-existent dislocation [22]. For example, in a situation where the pre-existent dislocation is one of chaotically distributed dislocations in a crystal, R is commonly close to the mean interspacing between dislocations of the ensemble [22].)

The splitting of the pre-existent dislocation into an ensemble of partial dislocations with small Burgers vectors (figure 5) is, in fact, a local transformation which does not affect the long-range stress field of the transformed defect configuration. In these circumstances, the screening length of stress fields of the partial dislocations is the same as with the pre-existent dislocation and the energy density $\tilde{W}_r$, the sum of proper elastic energy densities of the resultant dislocations, can be approximately defined as the energy density of the elastic distortions created by the pre-existent dislocation in the region outside of its amorphous core. That is

$$\tilde{W}_r \approx \frac{GB^2}{4\pi(1-\nu)}\ln\frac{R}{r} \tag{15}$$

where r denotes radius of the amorphous dislocation core.

Now let us examine $\tilde{W}_{d-d}$ in the first approximation, in which the dislocation ensemble resulted from the amorphizing splitting is characterized by a dislocation density continuously and homogeneously distributed along the cylinder-like interface between the amorphous region and the surrounding crystalline phase. In doing so, after some algebra (see appendix B), we find with the help of formulae [22] the energy density $\tilde{W}_{d-d}$ as follows:

$$\tilde{W}_{d-d} = \frac{GB^2}{4\pi(1-\nu)}\left(0.5 - 2\pi^{-1} + \ln\frac{2R}{r} + \ln 2\right). \tag{16}$$

From formulae (13) and (14) we find the following formula for decrease $\Delta\tilde{W}^{el}$ in the elastic energy related to the amorphizing splitting (figure 5):

$$\Delta\tilde{W}^{el} = \frac{GB^2}{4\pi(1-\nu)}\left(\ln\frac{Ra}{4r^2} - 1.5 + 2\pi^{-1}\right). \tag{17}$$

$\Delta\tilde{W}^{el} < 0$ for a wide range of parameters of the system and this, therefore, causes the driving force for the amorphizing splitting.

Now let us turn to analysis of the energy densities $\tilde{W}_c$ and $\tilde{W}_{int}$. The free-energy density $\tilde{W}_c$ of the amorphous core of the split dislocation is approximately as follows:

$$\tilde{W}_c \approx \pi r^2 \varepsilon_{a-c} \tag{18}$$

where ε_{a-c} is the difference between the free-energy densities (per unit volume) of the amorphous and crystalline phases. As to $\tilde{W}_{int}$, following [24], the energy density of a crystal/glass interface per unit area of such interface is $\approx \kappa\varepsilon_{a-c}$, where κ denotes the characteristic spatial scale of structural inhomogeneities in the amorphous phase. As a corollary, the energy density $\tilde{W}_{int}$ of the crystal/glass interface which surrounds the split dislocation core per unit of the dislocation length is as follows:

$$\tilde{W}_{int} \approx 2\pi r\kappa\varepsilon_{a-c}. \tag{19}$$

Hereinafter we assume that the splitting of a pre-existent dislocation into a cylinder-like ensemble of dislocations (figure 5) at its initial stage occurs in a jump-like stage with the pre-existent dislocation core radius ($\approx a$) abruptly changing into the radius r' of the initial cylinder-like nucleus of the amorphous phase. In these circumstances, from formulae (17)–(19), we find that the total change $\Delta\tilde{W}$ in the free-energy density, related to the amorphizing splitting (figure 5) at its initial stage as

$$\Delta\tilde{W} \approx \frac{GB^2}{4\pi(1-\nu)}\left(\ln\frac{Ra}{4r'^2} - 1.5 + 2\pi^{-1}\right) + \pi r'^2\varepsilon_{a-c} + 2\pi r'\kappa\varepsilon_{a-c}. \tag{20}$$

The amorphizing splitting (figure 5) at its initial stage occurs as an energetically profitable transformation, if $\Delta W < 0$. When $\Delta W > 0$, the amorphizing splitting at is energetically forbidden.

In estimations of ΔW, we can get to two situations, as discussed in section 3: situation (1), with an 'ordinary' density of defects and chemical homogeneity, and situation (2), with a high density of defects and/or chemical inhomogeneities. In the 'ordinary' situation (situation (1)) $\varepsilon_{a-c} \approx$ from $(G/83)$ to $(G/63)$. Then, for the characteristic

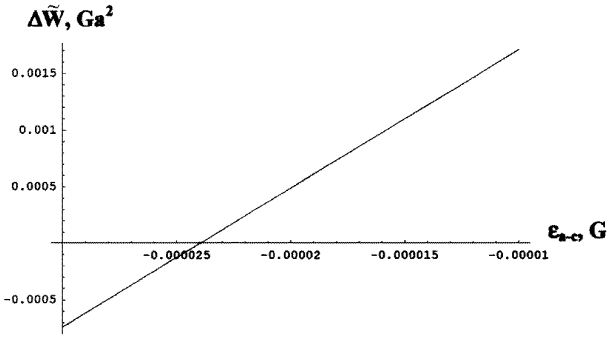

Figure 6. The dependence of $\Delta\tilde{W}$ on ε_{a-c}.

values of the parameters $r' \approx 3a$, $\kappa \approx 5a$, $\varepsilon_{a-c} \approx G/70$, $R = 10^3 a$, $B = a/10$ and $\nu = 1/3$, from formula (20) we find $\Delta\tilde{W} \approx 1.75G \times a^2 > 0$. As a result, the amorphizing splitting (figure 5) is energetically forbidden.

In situation (2) dealing, in particular, with irradiation-induced defects in the pre-existent crystalline phase (corresponding to experiments in [10]) as well as with the chemical composition changing in the vicinity of an interfacial dislocation due to intensive diffusion processes (corresponding to experiments in [11]), we have values of ε_{a-c} that are essentially lower than those in the 'ordinary' situation (situation (1)). With this taken into account, for the characteristic values of the parameters $r' \approx 3a$, $\kappa \approx 5a$, $R = 10^3 a$, $B = a/10$ and $\nu = 1/3$, from (20) we find dependence of $\Delta\tilde{W}$ on ε_{a-c}, which is shown in figure 6. $\Delta W(\varepsilon_{a-c}) < 0$ in some ranges of the parameters (see figure 6). Therefore, the amorphizing splitting (figure 5) at its initial stage is energetically profitable in the cases with the parameters valued in such ranges.

Now let us turn to the analysis of further continuous amorphizing splitting, which comes into play after the amorphous core of the split dislocation has been initially formed in the jump-like way. The splitting occurs continuously and is characterized by a continuous change (increase) of the amorphous core radius r. In these circumstances, the driving force for the amorphizing splitting, related to the corresponding decrease $\Delta\tilde{W}^{el}$ in the elastic energy, is defined as follows:

$$\tilde{F}^{el} = -\frac{\mathrm{d}\Delta\tilde{W}^{el}}{\mathrm{d}r} = \frac{Gb^2}{2\pi(1-\nu)}\frac{1}{r} \qquad (21)$$

$\tilde{F}_{el}$ decreases, as r increases. This, in the framework of our model, indicates that the effect of the dislocation-induced elastic distortions on nucleation of the amorphous phase decreases, when the amorphous nucleus grows at a dislocation (when the radius of the nucleus increases). This theoretical statement is in agreement with experimental data [10, 11] on the observation of amorphous nuclei at dislocations, that are characterized by finite dimensions.

5. Concluding remarks

Elastic distortions induced by intergranular boundaries and dislocations are theoretically revealed, here, to have a crucial influence on the nucleation of the amorphous phase at such boundaries and dislocations. In the framework of the suggested models, elastic-energy-decrease-induced transformations—splitting of grain boundaries (figures 1 and 3) and special splitting of lattice and interfacial dislocations (figure 5)—represent effective micromechanisms for the solid-state amorphization. In this context, grain boundaries and dislocations are theoretically recognized here as preferable places for nucleation of the amorphous phase; this corresponds to experimental data [7–11].

In general, the role of dislocations and grain boundaries in the amorphization process is not restricted to their capability to create stress fields, whose relaxation contributes to the driving of the solid-state amorphization. Diffusion in both dislocation cores and grain boundaries is essentially higher than that in the bulk crystalline phase [19]. This causes the effect of defects, dislocations, and grain boundaries on the solid-state amorphization to be different under at various conditions. So, diffusional mixing of atoms of different chemical species plays the important role in driving the solid-state amorphization in multilayer coatings and mechanically alloyed powders [1–6], in which case high diffusional properties of both dislocations and grain boundaries facilitate nucleation of the amorphous phase at such defects. At the same time, irradiation-induced point defects (whose generation in the pre-existent crystalline phase leads to the solid-state amorphization) intensively annihilate moving along dislocations and grain boundaries, in which case high diffusional properties of dislocations and grain boundaries facilitate annihilation of irradiation-induced point defects and, therefore, hamper the amorphization processes. (A similar effect occurs in irradiated nanocrystalline solids in which an extremely high density of grain boundaries, in many cases, provides the extremely fast annihilation of irradiation-induced point defects [27].)

New dislocations and grain boundaries are generated during plastic deformation [22, 28]. Therefore, the role of such defects increases in the amorphization processes occuring in plastically deformed materials. In this context, the effect of dislocations and grain boundaries, as preferable places for nucleation of the amorphous phase, can be naturally treated as the effect that significantly contributes to the experimentally observed [2] fact that the intensity of the amorphization processes in mechanically alloyed powders (where both deformation and diffusional mixing come into play) is more than that in multilayer coatings (where only diffusional mixing occurs). It should also be noted that irradiation is capable of causing changes in ensembles of dislocations and grain boundaries and, therefore, influencing the amorphization processes in irradiated crystals.

To summarize, as it has been theoretically shown, here, elastic distortions created by dislocations and grain boundaries play the significant role in the initiation of the solid-state amorphization at such defects. These results can be effectively used in a future (more complete) theoretical description of the amorphization at dislocations and grain boundaries, which should also take into account diffusion processes in dislocation cores and grain boundaries, as well as the (deformation- and/or irradiation-induced) evolution of ensembles of dislocations and grain boundaries.

Acknowledgments

Many thanks are due to Dr A L Kolesnikova for fruitful discussions. This work was supported, in part, by the Russian Foundation of Basic Researches (grant 98-02-16075) and by the Office of the US Naval Research (grant N00014-99-1-0569).

Appendix A

Surface S at which a displacement jump (associated with a dislocation) occurs is defined in the framework of the Volterra's scheme of introducing of dislocations in a solid as follows (for details, see [22, 23]): (1) a solid is cut along a surface S bounded by dislocation line; (2) one of the sides of the cut is displaced by vector $\boldsymbol{b}$, in which case either an excess or a deficit of material is formed in the region near the surface S; and (3) the sides of the cut are 'glued', in which case either the excess of material is removed or the deficit of material is compensated for by the addition of new material. Stages (1)–(3) result in the formation of a dislocation with Burgers vector $\boldsymbol{b}$, characterized by the surface S.

Appendix B

The discussed dislocation system in its final state represents a cylinder-like ensemble of dislocations with small Burgers vectors (figure 5). To analytically calculate the energy density $\tilde{W}_{d-d}$ of their interaction, we will model such dislocations to be uniformly and continuously distributed along the cylinder. The energy density of the interaction of two elemental (infinitesimal) fragments, say fragments 1 and 2, of the 'dislocation cylinder' (figure 5) can be written with the help of standard formula [22] as:

$$W_{12} = -\frac{G\,\mathrm{d}b_1\,\mathrm{d}b_2}{2\pi(1-\nu)}\left(\ln\frac{2r|\sin(\phi/2)|}{R} + \sin^2\frac{\phi}{2}\right) \qquad \text{(B1)}$$

where ϕ is the angle between normals to the fragments 1 and 2. Since $\int_0^{2\pi}\mathrm{d}b = B$, we find $\mathrm{d}b = (B/2\pi)\,\mathrm{d}\phi$. Integral of W_{12} (see formula $(B1)$) over the cylindrical region gives formula (16) for $\tilde{W}_{d-d}$.

References

[1] Johnson W L 1988 *Mater. Sci. Eng.* **97** 1–13
[2] Schultz L 1988 *Mater. Sci. Eng.* **97** 15-23
[3] Schwarz R B 1988 *Mater. Sci. Eng.* **97** 71–8
[4] Samwer K 1988 *Phys. Rep.* **161** 1–41
[5] Shingu P H and Ishihara K N 1995 *Mater. Trans. (Japanese Institute of Materials)* **36** 96–101
[6] Ovid'ko I A 1991 *Defects in Condensed Media: Glasses, Crystals, Quasicrystals, Liquid Crystals, Magnetics, Superfluids* (St. Petersburg: Znanie) (in Russian)
[7] Samwer K, Schroder H and Pampus K 1988 *Mater. Sci. Eng.* **97** 63–8
[8] Hollanders M A, Thijsse B J and Mittemejer E J 1990 *Phys. Rev.* B **42** 5481–94
[9] Gong W L, Wang L M and Ewing R C 1997 *J. Appl. Phys.* **81** 2570–4
[10] Cherns D, Hutchinson J L, Jenkins M L, Hirsch P B and White S 1980 *Nature* **287** 314–16
[11] Duscher G, Mullejans H, Werner J and Ruhle M 1996 *Mater. Sci. Forum* **207–9** 713–16
[12] Gutkin M Yu and Ovid'ko I A 1994 *Phil. Mag.* A **70** 561–75
[13] Osipov A V and Ovid'ko I A 1992 *Appl. Phys.* A **54** 517–19
[14] Ovid'ko I A 1991 *J. Phys. D: Appl. Phys.* **24** 2190–5
[15] Gutkin M Yu, Ovid'ko I A and Meshcheryakov Yu I 1993 *J. Physique* III **3** 1563–79
[16] Ovid'ko I A 1994 *J. Phys. D: Appl. Phys.* **27** 999–1007
[17] Ovid'ko I A and Osipov A V 1997 *Tech. Phys.* **42** 748–51
[18] Benedictus R, Bottger A and Mittenmejer E J 1996 *Phys. Rev.* B **54** 9109–19
[19] Sutton A P and Balluffi R W 1995 *Interfaces in Crystalline Materials* (Oxford: Clarendon)
[20] Nazarov A A, Valiev R Z and Romanov A E 1994 *Solid State Phenom.* **35/36** 381–6
[21] Mikaelyan K N, Ovid'ko I A and Romanov A E 1999 *Mater. Sci. Eng.* A **259** 132–7
[22] Hirth J P and Lothe J 1968 *Theory of Dislocations* (New York: McGraw-Hill)
[23] Mura T 1968 *Advances in Material Research* vol 3, ed H Herman (New York: Interscience) **3** 1–108
[24] Ovid'ko I A 1999 *Phil. Mag. Lett.* **79** 709–13
[25] Morris R G 1979 *J. Appl. Phys.* **50** 3250–2
[26] Gutkin M Yu, Ovid'ko I A and Romanov A E 1994 *Rad. Eff. Def. Solids* **129** 239–55
[27] Rose M, Gorazawski G, Miehe G, Ballogh A G and Hahn H 1995 *Nanostruct. Mater.* **6** 731–4
[28] Valiev R Z, Alexandrov I V and Islamgaliev R K 1998 *Nanostructured Materials: Science and Technology* ed G M Chow and N I Noskova (Dordrecht: Kluwer) pp 121–42